Journal of Power Sources 256 (2014) 264–273

Contents lists available at ScienceDirect

Journal of Power Sources

journal homepage: www.elsevier.com/locate/jpowsour

Supercapacitors based on modified graphene electrodes with poly(ionic liquid)

João Paulo C. Trigueiro, Rodrigo L. Lavall, Glaura G. Silva*

Departamento de Química, Universidade Federal de Minas Gerais, Av. Antônio Carlos, 6627 – Pampulha, CEP 31270-901 Belo Horizonte, MG, Brazil

HIGHLIGHTS

- The PIL:RGO electrode increases the compatibility with the ionic liquid electrolyte.
- The use of polymer PILTFSI showed to be a promising strategy for capacitive devices.
- The PIL:RGO supercapacitor exhibits high capacitance and indication of good cycle stability.

GRAPHICAL ABSTRACT

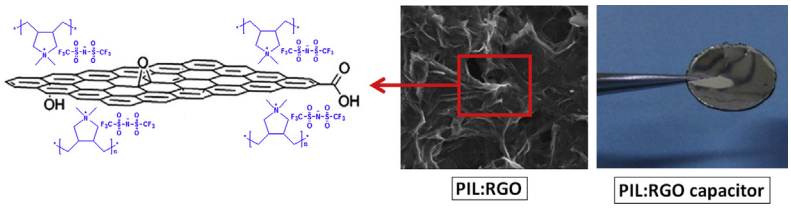

ARTICLE INFO

Article history:
Received 6 September 2013
Received in revised form
17 January 2014
Accepted 18 January 2014
Available online 24 January 2014

Keywords:
Electrochemical double layer capacitors
Ionic liquids
Polymeric ionic liquid
Reduced graphene oxide
1-Methyl-1-propylpyrrolidinium
bis(trifluoromethylsulfonyl)imide

ABSTRACT

The improved accessibility of the electrolyte to the surface of carbon nanomaterials is a challenge to be overcome in supercapacitors based on ionic liquid electrolytes. In this study, we report the preparation of supercapacitors based on reduced graphene oxide (RGO) electrodes and ionic liquid as the electrolyte (specifically, 1-methyl-1-propylpyrrolidinium bis(trifluoromethylsulfonyl)imide or [MPPy][TFSI]). Two types of electrodes were compared: the RGO-based electrode and a poly(ionic liquid)-modified RGO electrode (PIL:RGO). The supercapacitor produced with the PIL:RGO electrode and [MPPy][TFSI] showed an electrochemical stability of 3 V and provided a capacitance of 71.5 F g^{-1} at room temperature; this capacitance is 130% higher with respect to the RGO-based supercapacitor. The decrease of the specific capacitance after 2000 cycles is only 10% for the PIL:RGO-based device. The results revealed the potential of the PIL:RGO material as an electrode for supercapacitors. This composite electrode increases the compatibility with the ionic liquid electrolyte compared to an RGO electrode, promoting an increase in the effective surface area of the electrode accessible to the electrolyte ions.

1. Introduction

In supercapacitors (also known as electrochemical double layer capacitors), the electric charge is accumulated in a double layer, mainly by electrostatic forces, without any chemical change in the electrode materials [1,2]. Energy storage is based on the separation of charged species in the double layer formed on the electrode/electrolyte interface [3,4]. Supercapacitors have attracted much attention in recent years due to their important characteristics, such as high capacitance, high power density (~10 kW kg^{-1}), medium energy density (~5 Wh kg^{-1}) and a large number of life cycles (>100,000). One further advantage is that they can be fully charged or discharged in a few seconds [5]. These devices have a high power density and a relatively large energy density compared to conventional capacitors, which enables their application to energy storage systems [6]. Supercapacitors may complement or replace batteries where high power densities are required for short time intervals [7].

To generate high capacitance, the specific surface area of the electrode material must be as high as possible to accommodate a large number of ions at the electrode/electrolyte interface, promoting the capacitance of the electrical double layer [8,9]. Among the different materials studied for application as the electrodes of

* Corresponding author. Tel.: +55 (31) 34095768; fax: +55 (31) 34095711.
E-mail addresses: joaopcampos@yahoo.com.br (J.P.C. Trigueiro), rodrigollavall@gmail.com (R.L. Lavall), glaurasilva@yahoo.com, glaura@qui.ufmg.br (G.G. Silva).

0378-7753/$ – see front matter © 2014 Elsevier B.V. All rights reserved.
http://dx.doi.org/10.1016/j.jpowsour.2014.01.083

supercapacitors, carbon materials in a variety of forms (for example, carbon nanotubes, carbon felts and activated carbon) have been widely investigated. However, there are many possibilities for great advances in the characteristics of supercapacitors and the discovery of graphene has become an important event in this context.

Graphene is a single atomic layer of sp^2 carbon atoms and is a promising material for supercapacitors electrodes due to its fascinating physical and chemical properties [10,11]. Supercapacitors based on graphene materials and aqueous electrolytes have been produced, and the results show great potential for this new class of carbon material for high-performance devices [12,13]. Du et al. developed electrodes with free standing graphene nanosheets that were prepared using a coating method that exhibited a stable specific capacitance of 150 F g^{-1} in KOH aqueous solution (30 wt.%) as the electrolyte [14]. Recently, Sun et al. fabricated a supercapacitor using reduced graphene oxide paper synthesized using a flame-induced reduction; this supercapacitor had a specific capacitance of 212 F g^{-1} in 2 mol L^{-1} of KOH electrolyte [15].

A critical factor influencing the properties of a supercapacitor is the characteristics of the electrolyte. Organic electrolytes provide a greater potential window when compared to aqueous electrolytes. However, organic electrolytes have the drawback of low thermal stability and toxicity, which limits their use in supercapacitors [16].

Ionic liquids (IL), i.e., molten salts with melting points below 100 °C, have been intensively used as the electrolyte in various electrochemical systems, including supercapacitors because IL have unique physicochemical properties such as high thermal and chemical stability, low vapor pressure and a wider electrochemical stability window [17,18].

Extending the temperature range of the operation of supercapacitors is of great importance because supercapacitors can address the problems associated with operating in severe conditions, which is required for automotive, aerospace and power electronic applications. In this scenario, ionic liquids have an advantage because they are able to operate in high temperature extremes, which is not possible with conventional electrolytes.

Recent research has shown that the performance of supercapacitors using graphene with ionic liquids as the electrolyte may be improved [19,20]. In order to do this improvement is crucial enhance the accessibility of electrolyte ions at the electrode. A major challenge to overcome is the production of electrode materials based on graphene that can sustain high wettability with ionic liquid electrolytes. This may be accomplished by modifying the surface of the graphene.

Tamailarasan et al. developed a high-performance supercapacitor based on a multi-walled carbon nanotube, exfoliated graphene and a 1-butyl-3-methylimidazolium bis(trifluoromethylsulfonyl)imide ionic liquid ternary nanocomposite electrode; the same ionic liquid was used as the electrolyte [21]. Their study showed extremely high specific capacitance (201 F g^{-1}) for an ionic liquid-based device at a large specific current density of 2 A g^{-1}. The authors attributed the high performance of the device mainly to the presence of a layering of ionic liquid in the electrode material, forming a solid-like ionic liquid modifier to the carbonaceous surface. This layer of ionic liquid was supposed to enhance the electrolyte accessibility and facilitate ionic transport because it increases the number of ion diffusion paths inside electrode. In another study conducted by Kim et al., an interesting approach applying poly(1-vinyl-3-ethylimidazolium) bis(trifluoromethylsulfonyl)imide to modify the reduced graphene oxide electrodes was developed; these authors used the ionic liquid 1-ethyl-3-methylimidazolium bis(trifluoromethylsulfonyl)imide to prepare the supercapacitors [22]. This work also reported outstanding values for an ionic liquid-based supercapacitor. Capacitance values between 127 and 187 F g^{-1} were obtained depending on the applied current density. The authors believe that the wettability of the electrodes with an ionic liquid electrolyte was facilitated by the poly(ionic liquid) molecules electrostatically linked on the reduced graphene oxide surface, producing the high specific capacitance values.

In the present study, we employed a simple synthetic procedure for preparation of a polymeric ionic liquid and incorporation into a dispersion of reduced graphene oxide in dimethylformamide. From this dispersion, composite electrodes were prepared by the dripping technique, allowing control over the amount of deposited material to obtain self-supported films, which were used in the construction of a supercapacitor with ionic liquid as an electrolyte.

2. Experimental section

2.1. Materials

The ionic liquid 1-methyl-1-propylpyrrolidinium bis(trifluoromethylsulfonyl)imide [MPPy][TFSI] with 99% purity and water content of less than 100 ppm (according to the supplier) was purchased from Iolitec (Germany) and was used as it was received. Other physicochemical properties for this ionic liquid are summarized in Table 1 (Supporting information), according to the literature data [23]. Handling of the ionic liquid was performed in a glove bag under a nitrogen atmosphere. Lithium bis(trifluoromethylsulfonyl) imide (LiTFSI, 99.9%) and poly(diallyldimethylammonium) chloride solution (average Mw 400,000–500,000, 20 wt.% in H_2O) (PILCl) were obtained from Aldrich, Brazil. Natural graphite was purchased from Bay Carbon Co, USA.

2.2. Preparation of graphene oxide

Graphene oxide (GO) powder was prepared from natural graphite by an improved method (based on Hummers' method) according to the methodology previously reported in the literature. This method for producing GO has significant advantages over Hummers' method [24].

2.3. Preparation of chemically reduced graphene oxide

Hydrazine monohydrate was used as the reducing agent for production of RGO in a stoichiometric ratio of 1 μL of hydrazine to 3 mg of GO [25]. In a typical procedure, 150 mg of GO was dispersed in 50 mL of water with the aid of an ultrasound bath for 3 h, yielding a homogeneous yellow-brown dispersion (3 mg mL^{-1} of GO). Hydrazine monohydrate was subsequently added to the suspension, and the mixture was stirred at 80 °C for 12 h resulting in a black precipitate of RGO powder. The synthesized RGO was washed with water to remove excess hydrazine and dried in a vacuum oven at 60 °C for 12 h.

2.4. Synthesis of polymeric ionic liquid

The polymeric ionic liquid or poly(ionic liquid) (PIL) containing pyrrolidinium cation and bis(trifluoromethylsulfonyl)imide anion was synthesized by anion exchange reactions using a commercially available polymer poly(diallyldimethylammonium) chloride according to a procedure described in the literature [26]. Briefly, a solution of 8.52 g of LiTFSI salt in 10 mL of distilled water and a solution of 4 g of PILCl in 100 mL of distilled water were mixed for 5 min at room temperature to facilitate the exchange reaction of Cl^- ions by $TFSI^-$. After stirring, the resulting white solid (named PILTFSI) was separated by filtration and dried in a vacuum oven at 60 °C for 12 h until it reached constant weight.

2.5. Preparation of the supercapacitor electrodes

Two stable dispersions of RGO in dimethylformamide (DMF) were prepared with the assistance of a low-power ultrasonic bath for 3 h (30 mg of RGO in 100 mL of DMF). Afterward, 100 mg of PILTFSI was added to one dispersion, and the system was stirred until the polymer was completely dissolved. The suspensions with and without polymer were named PIL:RGO and RGO respectively. Then, both resulting dispersions (PIL:RGO and RGO) were deposited onto aluminum current collectors (Al sheet, thickness of 0.025 mm, 99.0%, Good Fellow) by drop casting until the full coverage of the electrode area. A mass of RGO between 10 and 50 μg was deposited on both types of electrodes, depending on the amount of dispersion dripped. Thus, one of the electrodes was formed by RGO only (called the RGO electrode) and the other consisted of a mixture of RGO and PILTFSI (named the PIL:RGO electrode). Each electrode had a circular area of 1.1 cm^2 (Supporting information, Fig. S1).

Supercapacitors were prepared in a stacked configuration with the electrodes of the carbon nanomaterials RGO or PIL:RGO (in contact with the Al sheets as current collectors), using a glass fiber membrane (MN GF-6, Macherey-Nagel) as the separator and the [MPPy][TFSI] ionic liquid as the electrolyte. A paper disk separator soaked with ionic liquid was sandwiched between the two electrodes.

2.6. Characterization of materials

The thermal characterization of carbon nanomaterials (GO and RGO), ionic liquid ([MPPy][TFSI]) and polymer samples (PILTFSI and PILCl) were obtained by thermogravimetric analysis (TGA). Measurements were performed under a nitrogen flow (25 mL min^{-1}) using a TA Instruments TGA Q5000. The samples were heated from room temperature to 1000 °C at 5 °C min^{-1}.

A Thermo Scientific spectrophotometer (model Nicolet 380 FT-IR) equipped with a Horizontal Attenuated Total Reflectance (HATR) accessory was used to acquire all spectra in the infrared range. The spectra of GO, RGO, PILTFSI, PILCl and PIL:RGO were recorded in the range of 4000–650 cm^{-1}.

The chemical composition of the PIL:RGO electrode was investigated by energy-dispersive X-ray spectroscopy (EDS) using an FEI QUANTA 200 microscope. EDS mapping was performed to analyze the distribution of the polymer on the surface of the electrode.

Zeta potential values of the RGO and PIL:RGO dispersions were measured using a Zetasizer Nano-ZS (Malvern Instruments, U.K.). The reported values are the average of 10 measurements. To perform the measurements, two RGO dispersions were prepared separately in dimethylformamide (DMF) with the aid of an ultrasound bath for 3 h (30 mg of RGO in 100 mL de DMF). Next, 100 mg of PILTFSI was added to one dispersion, and the system was stirred until complete dissolution of the polymer. Both resulting dispersions were analyzed.

Atomic force microscopy (AFM) measurements were performed in an Asylum Research MFP-3D-AS operated in the tapping mode. The AFM sample preparation was conducted by dispersing the GO powder in water using a low-power ultrasonic bath. Drops of the dispersion were deposited onto a silicon wafer.

The morphology of the carbon nanomaterial-based electrode was studied by scanning electron microscopy (SEM). Images were obtained with a field emission gun scanning electron microscope (FEI QUANTA 200) without any cover over the samples. The electrodes were analyzed directly on their respective substrates.

Electrochemical measurements were performed on a potentiostat/galvanostat Autolab PGSTAT30 (Eco Chemie). The electrical conductivity of ionic liquid was obtained from electrochemical impedance spectroscopy (EIS) in the frequency range from 1 MHz to 0.1 Hz at an open circuit potential (OCP) with an ac perturbation of 10 mV. The electrochemical stability window of LI was performed by linear sweep voltammetry (LSV) at 5 mV s^{-1}. A silver wire was used as a pseudo-reference electrode. The anodic and cathodic processes were scanned separately from the OCP.

The electrochemical capacitors were studied by electrochemical impedance spectroscopy, cyclic voltammetry (CV), and galvanostatic charge/discharge tests. Cyclic voltammetry experiments were performed at different scan rates of 10, 30, 50, and 80 mV s^{-1} in a voltage range of −1.5 to 1.5 V. The EIS measurements were conducted in a frequency range of 1 MHz to 0.01 Hz at the OCP with an ac perturbation of 10 mV. The EIS and CV were performed at 25 and 60 °C. Galvanostatic charge/discharge curves were obtained by applying a current density of 0.2 A g^{-1} in a voltage range of 0–2 V. Measurements were performed at 25 °C and over 2000 cycles.

3. Results and discussion

3.1. Ionic liquid and poly(ionic liquid) characterization

The characterization of [MPPy][TFSI] ionic liquid was performed prior to its use as the electrolyte in the supercapacitors to evaluate its thermal stability, conductivity and electrochemical stability window as an electrolyte.

Thermogravimetric measurements (Supporting information, Fig. S2) showed that [MPPy][TFSI] is thermally stable up to 335 °C with a weight loss of less than 0.3% until the beginning of its degradation, demonstrating the high thermal stability and level of purity of this ionic liquid.

Impedance spectroscopy was applied to investigate the ionic liquid conductivity in the range of 25–105 °C. The Arrhenius plot presented in Fig. 1a shows that the conductivity of the sample is strongly dependent on temperature because the value increases linearly with an increase in temperature from 25 to 105 °C. A conductivity value of 4.2 mS cm^{-1} was observed for [MPPy][TFSI] at room temperature and reaches the value of 10.3 mS cm^{-1} at 105 °C. Previous reports applying different classes of ionic liquids as electrolytes in supercapacitors found lower conductivity results compared to those obtained in our study [16,18,20]. This demonstrates the potential of [MPPy][TFSI] for use as an electrolyte in supercapacitors.

Linear sweep voltammetry measurements were used to evaluate the electrochemical stability window of [MPPy][TFSI] (Fig. 1b). The E_{red} and E_{ox} were defined as the potential where the limit current density reached 0.1 mA cm^{-2}. The electrochemical window between the E_{red} and E_{ox} was 3.5 V. The result obtained here is in agreement with other studies in the literature on LI showing the absence of water during the manipulation and measurement conditions [17]. The electrochemical performance of LI depends on the nature of both the cation and anion, but the amount of water present in the sample is also a very important factor to achieve a wide range of stability. The increase in the amount of water significantly reduces the electrochemical stability of an ionic liquid [27].

Different types of poly(ionic liquid)s have been synthesized in literature, using two main strategies: direct polymerization of monomers of ionic liquids [28] and polymerization of a monomer followed by an anion exchange reaction directly in the synthesized PIL [26]. Generally, the second strategy is accompanied by precipitation of new polymer because of its insolubility in water (in this case, a halide anion is replaced by another anion that makes the polymer hydrophobic) [26]. This strategy was used in this work for the synthesis of poly(ionic liquid).

The anion exchange reaction was performed in a commercially available pyrrolidinium-based polymer, poly(diallyldimethylammo

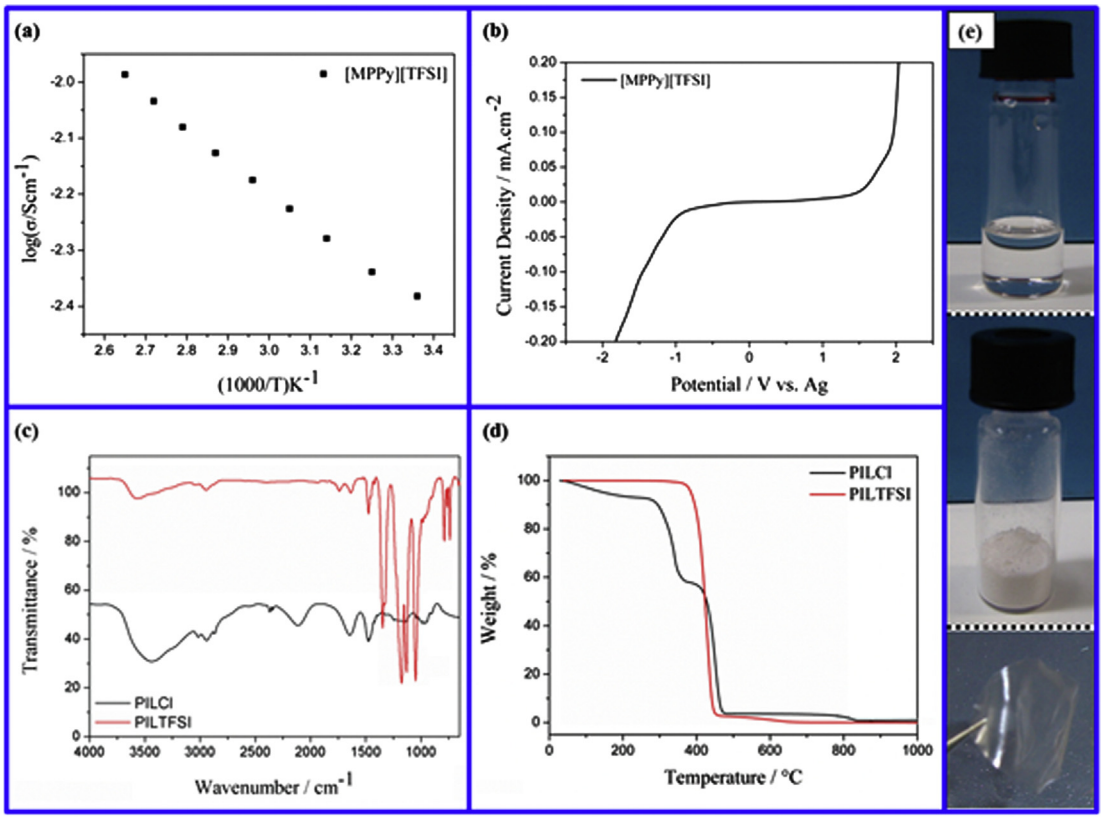

Fig. 1. Arrhenius plot (a) and linear sweep voltammogram (b) for 1-methyl-1-propylpyrrolidinium bis(trifluoromethylsulfonyl)imide [MPPy][TFSI]. Infrared spectra (c) and TGA curves (d) for PILCl and PILTFSI. Ionic liquid [MPPy][TFSI], the solid PILTFSI synthesized, and a free-standing polymeric film of PILTFSI (from top to bottom) (e).

nium) chloride. The replacement of the Cl^- anion by the $TFSI^-$ anion, which has a hydrophobic character, renders the synthesized new polymer insoluble in water, and their precipitation in the form of a white solid occurred as soon as the reagents were mixed. This reaction showed a high yield (89%) and is simple to perform.

The synthesized polymer was characterized by TGA and infrared. Fig. 1c shows the infrared spectra of the PILCl and PILTFSI polymers. The spectra show the main bands observed in the literature for the two polymer samples [26]. The bands corresponding to the structure of the cation (the basis of the polymeric chain of two polymers) were observed in both spectra, mainly between 3100 and 2900 cm^{-1} (assigned to the C—H stretch), at 1640 (the C—N stretch) and 1476 cm^{-1} (the C—H deformation). After the anion exchange reaction, new bands attributed to TFSI were observed at 1049, 1130, 1174 cm^{-1} (all assigned to the S═O stretch) and 1346 cm^{-1} (the C—F stretch) [26].

The TGA curves for PILCl and PILTFSI are shown in Fig. 1d. As observed, the polymers present different thermal behaviors because the thermal stability of this polymer class depends strongly on the type of anion present in the structure. Moreover, the difference in thermal behavior indicates that the anion exchange reaction occurred satisfactorily.

The precursor polymer is highly hygroscopic, showing a weight loss of 7% in the temperature range up to 225 °C, which is most likely due to the removal of physisorbed water. The sample of PILCl presents a lower thermal stability than PILTFSI and decomposes in two steps. The PILTFSI is thermally stable up to 345 °C, decomposing completely in one step. Fig. 1e shows the ionic liquid [MPPy][TFSI] used on a supercapacitor, the solid synthesized PILTFSI and a free-standing film obtained by this polymer, which can be handled without difficulty (from top to bottom).

3.2. Carbon nanomaterials

AFM characterization is the most common method for the quantification of the degree of exfoliation from graphite to produce a single graphene sheet after the dispersion of the powder in a solvent. AFM images and the corresponding height profile of the GO are shown in Fig. 2a.

The AFM analysis confirmed that the thickness of these GO nanosheets is approximately 1.2 nm. In agreement with previous results, these graphene oxide layers should be mostly monolayered, whereas the overlapped regions typically have two or more layers [29–31]. The observed graphene oxide nanosheets thicknesses are significantly larger than the theoretical values of a graphene sheet (0.34 nm) due to the number of oxygenous groups linked on the surface of the GO nanosheets [32].

The thermogravimetric analysis has been used to qualitatively evaluate the degree of reduction achieved by the chemical treatment of GO with hydrazine. Fig. 2b shows the TGA curves for the GO and the RGO. GO shows a weight loss of 17% in the temperature range up to 110 °C, and this is related to the removal of physisorbed water. The significant weight loss of 40% from 110 to 300 °C is attributed to the decomposition of labile oxygen functional groups. A third weight loss occurs at a higher temperature and is related to the degradation of the GO nanosheets [30,33]. In contrast, RGO showed much lower weight loss than GO, indicating a significant decrease in the number of labile oxygen groups by the hydrazine reduction and the restoration of the conjugated π-rich network within the layers of the graphene [30,33].

The oxygenated functional groups are infrared active; thus, infrared spectra can also be used to indicate the degree of removal of the oxygen groups. The spectra of GO and RGO are shown in Fig. 2c. GO exhibited characteristic bands of hydrophilic oxygen groups

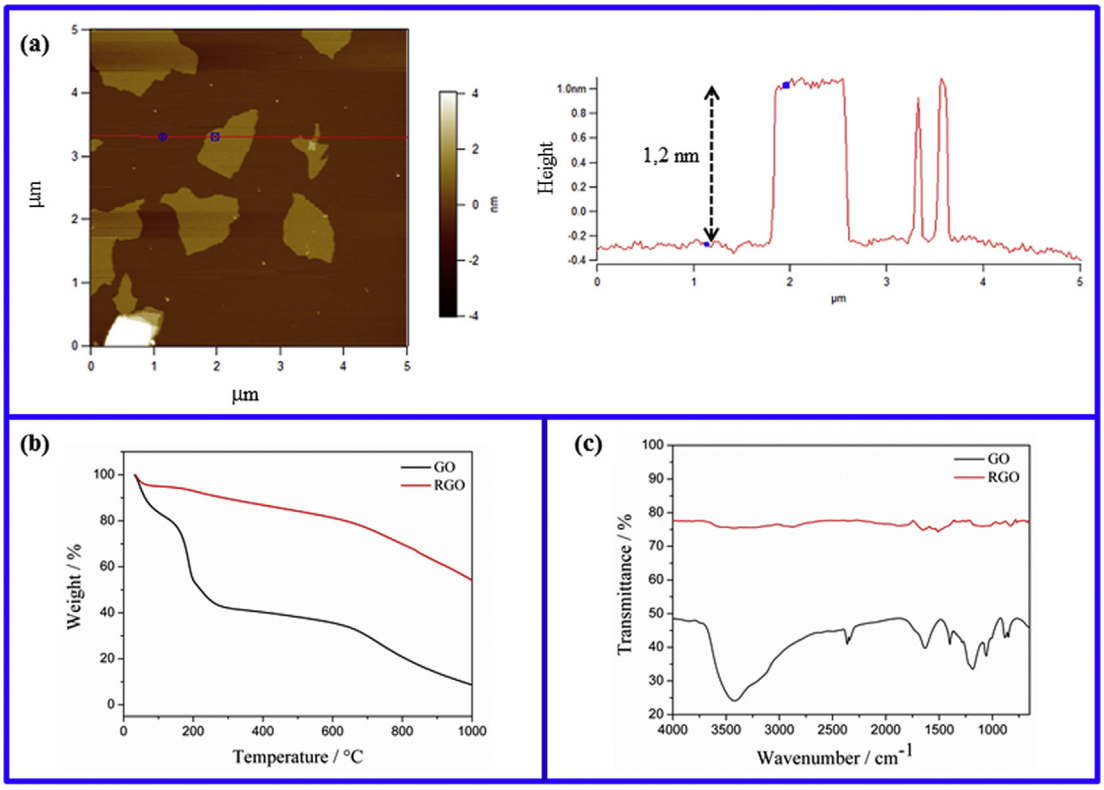

Fig. 2. AFM image of GO nanosheets on a silicon wafer with a corresponding line profile (a). TGA curves (b) and infrared spectra (c) for the GO and RGO nanomaterials.

mainly corresponding to O–H (the broad band at 3420 cm^{-1}), carbonyl (~1630 cm^{-1}), carboxylic acid (~1728 cm^{-1}) and C–O–C (~1057 cm^{-1}) stretching vibrations. The vibrational modes observed at 1400 cm^{-1} and 1180 cm^{-1} were assigned to the O–H and C–H deformations, respectively [34–36]. After the reduction by hydrazine, the decrease in the band's intensity indicates that a majority of functional groups have been removed. This result is in agreement with the observations by thermogravimetric analysis, which also indicated a satisfactory reduction by hydrazine.

3.3. Electrodes

The RGO and PIL:RGO dispersions were used for the production of carbon nanomaterial electrodes for the supercapacitors. The PIL:RGO material was composed of RGO nanosheets probably covered with PILTFSI molecules. The zeta potential values of the dispersions were measured before the addition of PILTFSI, and the value obtained was −38.3 mV, which is most likely due to the surface of the RGO nanosheets being negatively charged because the oxygenated groups were not fully reduced. In contrast, after the addition of PILTFSI, a reversal of the zeta potential to 71.4 mV occurred, suggesting that the negatively charged functional groups were covered and stabilized by the positively charged polycations on PILTFSI. In a similar work, Kim et al. used zeta potential to affirm that the solid films produced from RGO dispersions have been covered by the polymer [22].

The coating of the polymer on the RGO sheets most likely occurs because of the cation–π electrostatic interaction, in addition to the negative charge density on the oxygen function. Fig. 3a illustrates the interaction between the polymer and the RGO.

The surface of the PIL:RGO electrode was analyzed by EDS, and the data show that the polymer is impregnated on the surface of the RGO nanosheets because the observed peaks are due to the atoms that compose the PILTFSI shown in Fig. 3b. The EDS mapping for different atoms was obtained in the same sample and confirms that the polymer covers the RGO nanosheets homogeneously (Fig. 3c). The use of EDS to support the surface coverage conclusion has been applied in works with RGO/PIL and graphene-carbon nanotubes/solid-like ionic liquid [21,36]. In addition, infrared analysis was performed in PIL:RGO and PILTFSI films with the aid of a HATR accessory and we compared these results with the RGO infrared spectra (Supporting information, Fig. S3). It was verified the predominance of PIL characteristic bands in PIL:RGO film which indicates the covering.

The morphology of the RGO and PIL:RGO electrodes was investigated by SEM. Fig. 4(a, b) shows the surface and cross-sectional SEM images of the samples.

From the SEM images of the surface, a wrinkle-like morphology can be observed in both electrodes. In addition, it was verified that well-interconnected carbon nanomaterials, where the substrates are completely covered by the RGO nanosheets, result in a conductive carbon surface and are extremely important for achieving high capacitance values. The cross-sectional SEM image of PIL:RGO presents a favorable morphology for application in electrochemical capacitors because it displays a separated thin sheet with a single or few layered structures, promoting a high surface area accessible to the electrolyte ions. This suggests that the polymer molecules cover the surface of the RGO and most likely act as a spacer for the nanosheets, increasing the interlayer space.

3.4. Supercapacitors

The two-electrode system configuration was used to evaluate the performance of the supercapacitors, which is reported in terms of the mass of the active electrode materials. Two different capacitors were produced, one with RGO-based electrodes and one with PIL:RGO-based electrodes. The electrochemical properties of the different capacitors were studied by impedance spectroscopy, galvanostatic charge/discharge cycling and cyclic voltammetry measurements.

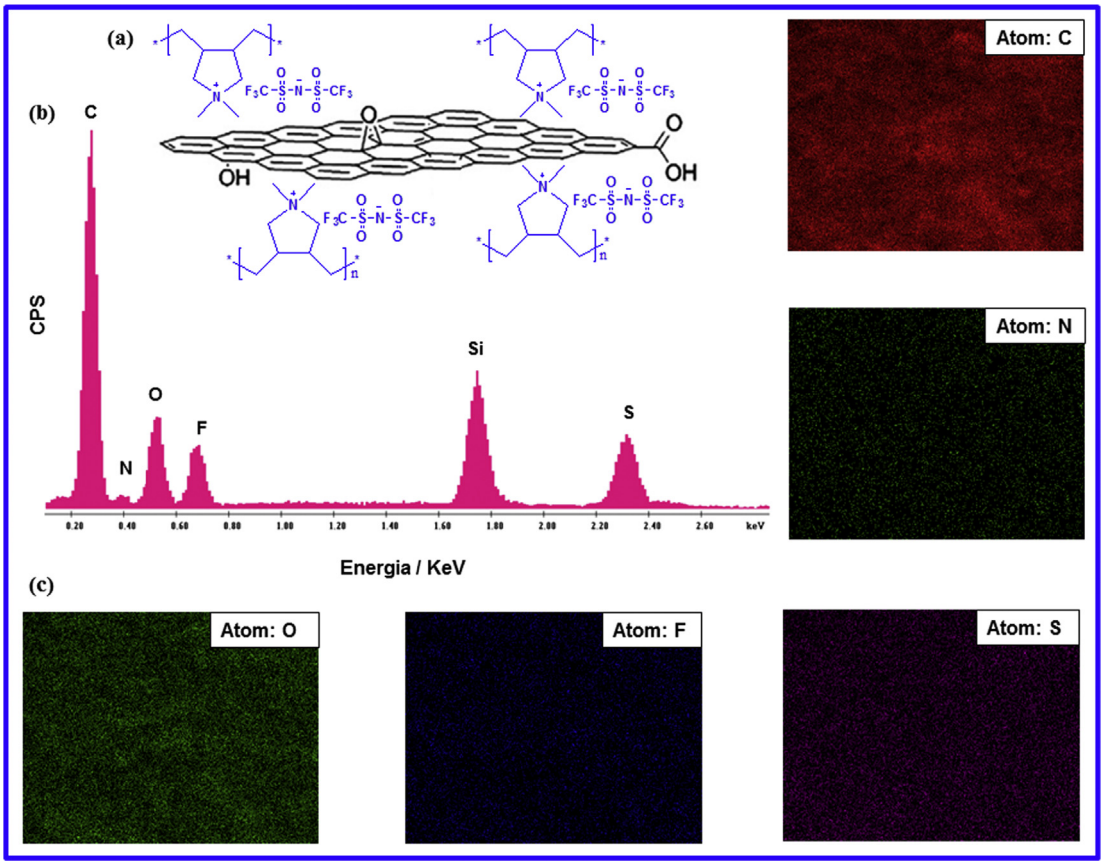

Fig. 3. Scheme for interaction between the cation of PILTFSI and the negatively charged RGO nanosheets (a). EDS spectra for the PIL:RGO electrode (b), EDS mapping (elements C, N, S, F and O) for the PIL:RGO electrode (c).

Fig. 5(a, b) shows the cyclic voltammograms for the supercapacitors at 25 °C. The CV curves for the RGO and PIL:RGO capacitors at all scan rates present a nearly rectangular shape which is associated with the capacitive behavior [2,37]. In fact, the voltammograms observed are typical of electrochemical capacitors prepared with carbon material having resistivity related to the functional groups not reduced with hydrazine (and those due to the polymer to the device with PIL:RGO) [2].

In the CV measurements conducted at 60 °C, the behavior was similar to the curves presented in Fig. 5a for all samples. The cell capacitance (C_{cell}) was calculated from the CV curves using Equation (1) and the best results were obtained for the scan rate of 10 mV s^{-1} [18,21,38].

$$C_{cell} = \frac{I}{dV/dt} \quad (1)$$

where C_{cell} is the capacitance of the cell in farad, I is the average current (A), dV/dt is the potential sweep rate (V s^{-1}). In a symmetrical system, due to the series capacitance formed in two-electrode system, the specific capacitance (C_{sp}) in farad per gram of active material is related to the capacitance of the cell according Equation (2) [18,21,38].

$$C_{sp} = \frac{2C_{Cell}}{m} \quad (2)$$

where m is the mass per electrode of active electrode material (g).

The RGO capacitor displays capacitance values of 17.0 and 20.2 F g^{-1} operating at 25 and 60 °C, respectively. The PIL:RGO capacitor showed a capacitance of 64.3 and 80.0 F g^{-1} at 25 and 60 °C, respectively. The PIL:RGO capacitor presented curves with areas slightly larger and, consequently, the capacitance values were higher than the RGO capacitor. The higher capacitance values observed for this capacitor are a consequence of the surface modification of the electrode by the PIL that renders it more accessible to the electrolyte ions than the RGO electrode.

The increase in capacitance as a function of temperature is due to the greater mobility of the ionic species. Recently, Borges et al. used a mixture of functionalized carbon nanomaterials to produce supercapacitors that use ionic liquid as the electrolyte. The devices were tested at 25, 60 and 100 °C, and the results showed an 8% increase in the specific capacitance when the device was operated at 100 °C [20]. This demonstrates the advantage of using the ionic liquid as the electrolyte in this device because it allows the capacitor to operate at high temperatures without losing its properties.

The Nyquist plots for the two capacitors at 25 and 60 °C are illustrated in Fig. 5(c, d). According to the data in the literature, the intersection of the curves at the real axis in the high frequency range represents the equivalent series resistances (ESR) of the electrodes; the ESR is a key parameter that influences the charge/discharge rate of the supercapacitor [6,11,39].

The value represents the total combination of the ionic resistance of electrolyte, the interfacial intrinsic resistance of the active electrode material and the interfacial resistance between the electrode and the current collector [15]. It can be noted from the Nyquist plots that the ESR decreases with temperature due to the increased mobility acquired by the ionic species. The ESR of the RGO capacitor were 11.0 Ω and 5.0 Ω at 25 and 60 °C, respectively; for the PIL:RGO capacitor, the ESR were 7.4 Ω and 5.0 Ω at 25 and

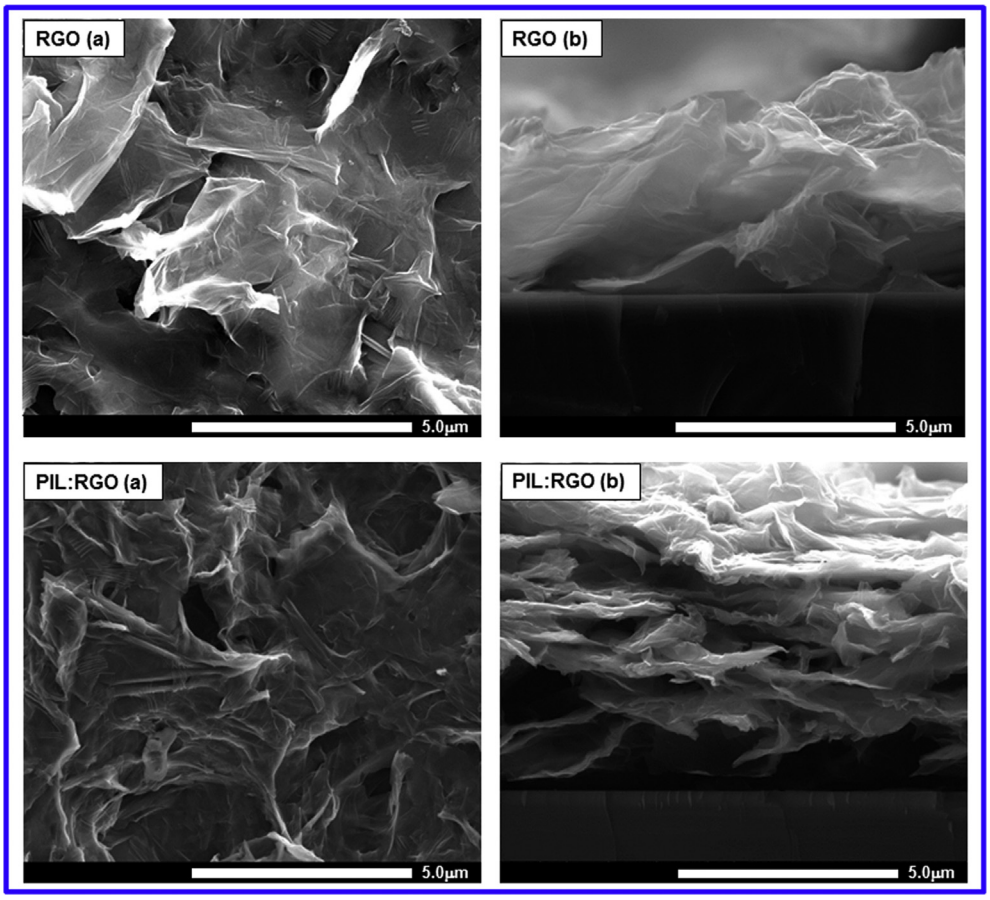

Fig. 4. SEM images of the RGO and PIL:RGO electrodes. Top-view (a) and cross-section (b) images.

60 °C, respectively. No significant differences were observed in the ESR values when the RGO and PIL:RGO capacitors are compared. This is important and shows that the addition of the PIL:TFSI polymer does not promote an increase in the electrical resistance of the system that would lead to a loss of performance. In addition, the capacitors exhibited low resistance values according to the CV data.

In the intermediate frequency region, the slope of the 45° portion of the curve is related to ion diffusion and transport in the electrolyte, usually called Warburg impedance [40,41]. In the systems studied, this phenomenon was not clearly observed for both the RGO and PIL:RGO capacitors, indicating that the ionic diffusion in the electrodes does not show a significant difference between them and that the ions can easily access the electrodes. Furthermore, at low frequency, the imaginary part of the impedance curves approaches a vertical line in both the RGO and PIL:RGO capacitors, which indicates a capacitive-type behavior, according to the CV results [42].

Rate capability is an important parameter in the development and application of supercapacitors. Fig. 6 shows the influence of different scan rates on the specific capacitances of PIL:RGO and RGO capacitors. The specific capacitance decreases gradually with increase of scan rate. Compared to RGO, the PIL:RGO capacitor not only displays higher specific capacitance values but also retains them well at high scan rates. The specific capacitance of PIL:RGO at 25 °C drops only 20% (from 64.3 to 51.6 F g^{-1}) as scan rate increases from 10 to 30 mV s^{-1}, while the RGO capacitor loses 42% of its capacitance (from 17 to 9.8 F g^{-1}) under the same conditions. This is equivalent to a capacity retention of 80 and 58% for PIL:RGO and RGO capacitors, respectively. When the capacitors are heated to 60 °C, the capacity retention is 70 and 61% for PIL:RGO and RGO-based supercapacitors, respectively.

The improvement of the rate capability of PIL:RGO capacitor can be attributed to the effective intercalation and distribution of PILTFSI molecules among RGO nanosheets, which contributes to an improvement in its wettability as well as interaction with the ionic liquid. Our results show a high rate capability for the devices prepared (especially for the PIL:RGO capacitor) when compared with other reported results for graphene electrodes [11,43].

Cycling performance is one of the most important properties for electrochemical capacitors. Galvanostatic charge–discharge experiments were performed at room temperature and at a current density of 0.2 A g^{-1} in the range 0–2 V to evaluate the stability of the capacitors. The galvanostatic charge–discharge was also used to obtain the specific capacitances of the different capacitors (Fig. 7a). All curves showed a slight voltage change at the beginning of the discharge state which is usually associated with IR drop of supercapacitors. The modest observed IR drop demonstrates that the both RGO and PIL:RGO capacitors has a small internal resistance and exhibit good efficiency [16,21,37].

The specific capacitance (C_{sp}) was calculated using the galvanostatic charge/discharge data according to Equations (1) and (2). In this case, I is the applied current (A) and dV/dt is the slope of the discharge curve in the Equation (1) (V s^{-1}) [18,21,38]. The term dV/dt was obtained according to the following equation [38]:

$$\frac{dV}{dt} = \frac{V_{max} - \frac{1}{2}V_{max}}{T_2 - T_1} \quad (3)$$

The specific capacitance was calculated to be 71.4 and 30.5 F g^{-1} for the PIL:RGO and RGO capacitors, respectively. These values show a great similarity with the results obtained by cyclic

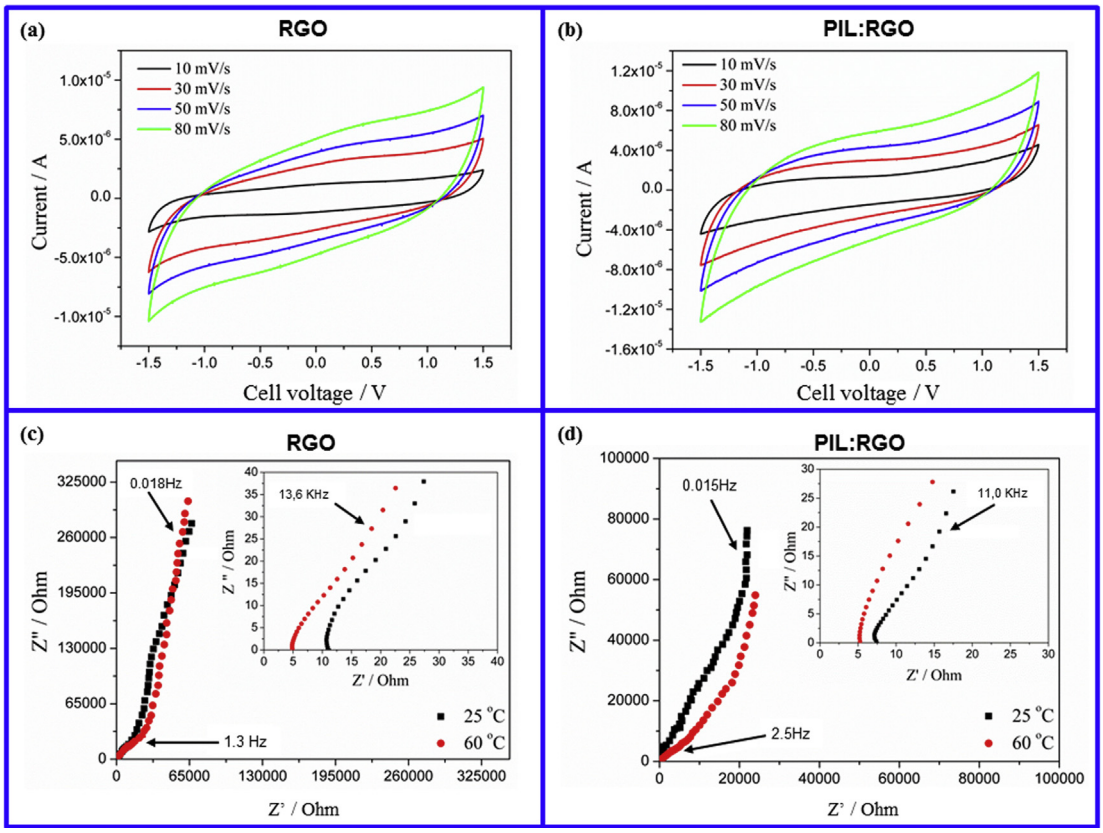

Fig. 5. Cyclic voltammograms for the RGO (a) and PIL:RGO (b) capacitors at different scan rates at 25 °C. Nyquist plots for the RGO (c) and PIL:RGO (d) capacitors at 25 and 60 °C. The insets show expanded regions of high frequency. Measurements were performed with a symmetrical cell with the two carbonaceous electrodes coated on aluminum current collectors and the ionic liquid impregnated in a glass membrane as separator.

voltammetry at 25 °C. Fig. 7b shows the variation in specific capacitance with the number of charge–discharge cycles for both capacitors at a voltage of 2 V. The RGO and PIL:RGO capacitors exhibited a high electrochemical stability after 2000 cycles of charge–discharge. The degradation of the specific capacitance after 2000 cycles is only 10% (for the PIL:RGO capacitor) and 14% (for the RGO capacitor), indicating that both devices show excellent cyclic stability. A larger number of cycles would be recommended for supercapacitors, however the experiments carried out in this work allow a first evaluation of device stability.

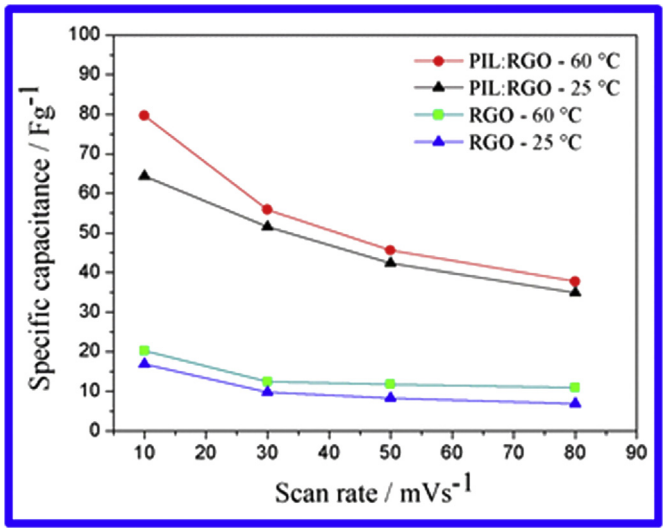

Fig. 6. Specific capacitances obtained from cyclic voltammograms of PIL:RGO and RGO-based supercapacitors at different scan rates at 25 and 60 °C.

Simultaneous high energy and power density is a goal that has been pursued in the supercapacitor field. It is known that the wettability of carbon materials by an electrolyte is one of the crucial factors that is require to facilitate significant advances in this direction, in addition to an increased operating voltage of the device, which is facilitated by the use of ionic liquid electrolytes. The energy density (E) and power density (P) were calculated according to Equations (4) and (5) [3,6].

$$E = \frac{1}{2} \cdot C_{sp} \cdot V^2 \tag{4}$$

$$P = \frac{V^2}{4 \cdot m \cdot R_{esr}} \tag{5}$$

where C_{sp} is the specific capacitance of the total cell, V is the maximum charging voltage, m is the total weight of the two electrodes and R_{esr} is the equivalent series resistance.

The PIL:RGO supercapacitor reached values as high as 2.1 kW kg^{-1} and 40.0 Wh kg^{-1} (for power and energy densities, respectively). These results can be further improved because they were obtained from the measured galvanostatic charge–discharge with the device operating at 2 V. This potential value is already high when compared to the values normally exhibited by capacitors using aqueous electrolytes; however, it is a value below the limit of electrochemical stability supported by ionic liquids (clearly, our ionic liquid supports up to 3 V without the presence of Faradaic

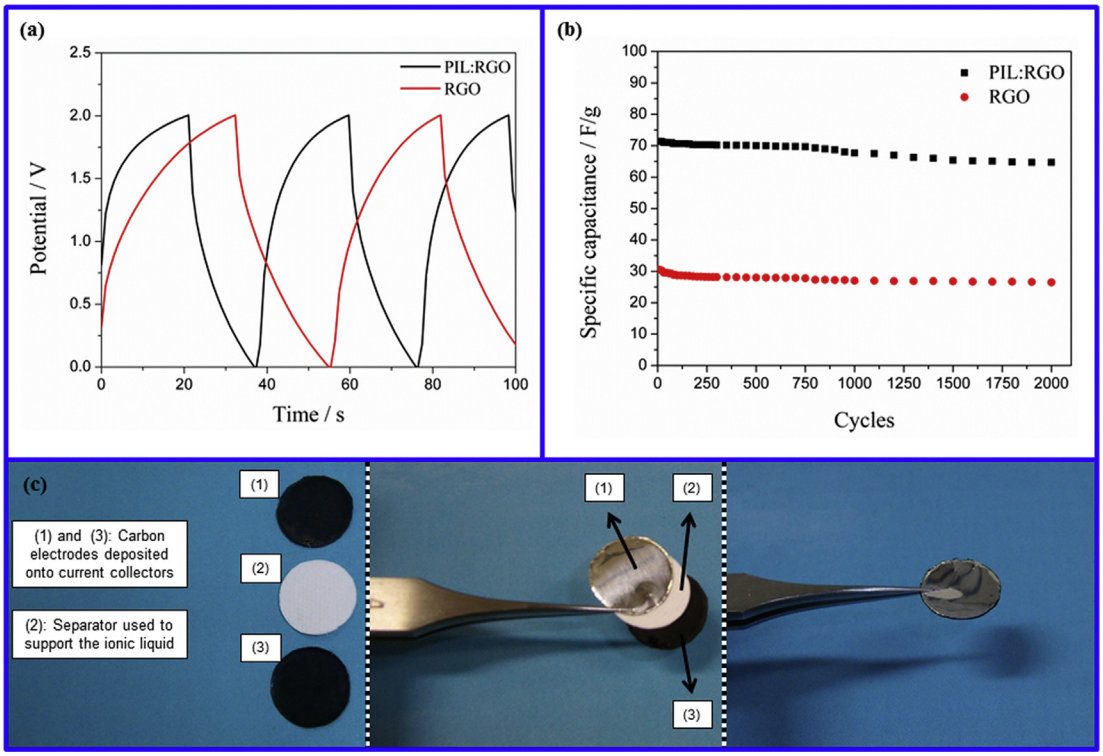

Fig. 7. Galvanostatic charge–discharge curves for RGO and PIL:RGO capacitors at 25 °C (current density: 0.2 A g^{-1}) (a). The specific capacitance change as a function of the number of charge–discharge cycles (b). Optical images of prototype supercapacitor developed in this work. From left to right: electrodes of carbon nanomaterials and the separator soaked with ionic liquid, the sequence used for the preparation of the device and the resulting device (c).

reactions in this potential window as in Fig. 1a). The results reported here are comparable to or higher than the values reported in previous studies [20,44]. In a work conducted by Balducci et al. using the *N*-butyl-*N*-methylpyrrolidinium bis(trifluoromethylsulfonyl)imide ionic liquid (which is very similar to the one used in this study), results of 2 kW Kg^{-1} and 20 Wh Kg^{-1} (for power and energy densities) were obtained in a cell operated at 3.5 V [18]. This demonstrates the good performance achieved by the PIL:RGO supercapacitor prepared in this work.

As mentioned in the introduction, the study developed by Kim et al. is the main reference for comparison of our results [22]. Although there were important differences between the two studies (e.g., a different procedure for the reduction of the graphene oxide, a distinct form of capacitor preparation and different classes of ionic liquid/poly(ionic liquid) employed in each work), the results are similar in the sense that the PIL contributes to a considerable increase in capacitance values, demonstrating the potential of this class of material for the surface modification of some carbon materials, such as graphene, and application in the preparation of electric double layer capacitors. The fact that the synthetic procedures and device assembly was simpler is an advantage of our approach.

4. Conclusions

The use of poly(ionic liquid) as a material component of supercapacitor electrodes proved to be a promising strategy for achieving high efficiency capacitive devices. A higher value of capacitance was obtained by the PIL:RGO capacitor in comparison with the RGO capacitor. This indicates that the PILTFSI polymer increases the compatibility of the RGO with the ionic liquid electrolytes and improves the accessibility of ions on a carbon nanomaterial surface due the similarity between the structure of the synthesized polymer and the ionic liquid electrolyte. Both the polymer and the ionic liquid have the same cation and anion with a hydrophobic nature.

The behavior of the specific capacitance values obtained in the device prepared in this work suggests that the wettability of the RGO electrodes with [MPPy][TFSI] ionic liquid was facilitated by the PILTFSI molecules electrostatically bonded onto the RGO surface. The polymer may increase the effective surface area accessible to the electrolyte ions, encouraging the formation of an enhanced electrical double layer at the electrode/electrolyte interface.

Acknowledgments

The authors are grateful to CNPq for the scholarship of João Paulo Campos Trigueiro and to Pró-Reitoria de Pesquisa – Universidade Federal de Minas Gerais (UFMG). The authors extend gratitude to Luis Carlos Oliveira da Silva (Departamento de Química/UFMG, Brazil) for the synthesis of the graphene oxide, to Professor Tulio Matencio (Departamento de Química/UFMG, Brazil) for the zeta potential measurements and for the images provided by the Centro de Microscopia-UFMG.

Appendix A. Supplementary data

Supplementary data related to this article can be found at http://dx.doi.org/10.1016/j.jpowsour.2014.01.083.

References

[1] I.V. Barsukov, C.S. Johnson, J.E. Doninger, V.Z. Barsukov, New Carbon Based Materials for Electrochemical Energy Storage Systems: Batteries, Supercapacitors and Fuel Cells, Springer, Dordrecht, 2006.
[2] E. Frackowiak, F. Béguin, Carbon 39 (2001) 937–950.

[3] B.E. Conway, Electrochemical Supercapacitors: Scientific Fundamentals and Technological Applications, Kluwer Academics and Plenum, New York, 1999.
[4] F. Béguin, E. Frackowiak, Carbons for Electrochemical Energy Storage and Conversion Systems, CRC Press, Boca Raton, 2010.
[5] A.G. Pandolfo, A.F. Hollenkamp, J. Power Sources 157 (2006) 11–27.
[6] Q. Cheng, J. Tang, J. Ma, H. Zhang, N. Shinya, L.C. Qin, Phys. Chem. Chem. Phys. 13 (2011) 17615–17624.
[7] R.Y. Lin, P.L. Taberna, S. Fantini, V. Presser, C.R. Perez, F. Malbosc, N.L. Rupesinghe, K.B.K. Teo, Y. Gogotsi, P. Simon, J. Phys. Chem. Lett. 2 (2011) 2396–2401.
[8] P. Simon, Y. Gogotsi, Nat. Mater. 7 (2008) 845–854.
[9] J.R. Miller, P. Simon, Science 321 (2008) 651–652.
[10] S. Stankovich, D.A. Dikin, G.H.B. Dommett, K.M. Kohlhaas, E.J. Zimney, E.A. Stach, R.D. Piner, S.T. Nguyen, R.S. Ruoff, Nature 442 (2006) 282–286.
[11] D. Zhang, T. Yan, L. Shi, Z. Peng, X. Wen, J. Zhang, J. Mater. Chem. 22 (2012) 14696–14704.
[12] Y. Wang, Z. Shi, Y. Huang, Y. Ma, C. Wang, M. Chen, Y. Chen, J. Phys. Chem. C 113 (2009) 13103–13107.
[13] M.D. Stoller, S. Park, Y. Zhu, J. An, R.S. Ruoff, Nano Lett. 8 (2008) 3498–3502.
[14] X. Du, P. Guo, H. Song, X. Chen, Electrochim. Acta 55 (2010) 4812–4819.
[15] D. Sun, X. Yan, J. Lang, Q. Xue, J. Power Sources 222 (2013) 52–58.
[16] K.K. Denshchikov, M.Y. Izmaylova, A.Z. Zhuk, Y.S. Vygodskii, V.T. Novikov, A.F. Gerasimov, Electrochim. Acta 55 (2010) 7506–7510.
[17] M. Galinski, A. Lewandowski, I. Stepniak, Electrochim. Acta 51 (2006) 5567–5580.
[18] A. Balducci, R. Dugas, P.L. Taberna, P. Simon, D. Plée, M. Mastragostino, S. Passerini, J. Power Sources 165 (2007) 922–927.
[19] D. Wei, T.W. Ng, Electrochem. Commun. 11 (2009) 1996–1999.
[20] R.S. Borges, H. Ribeiro, R.L. Lavall, G.G. Silva, J. Solid State Electrochem. 16 (2012) 3573–3580.
[21] P. Tamailarasan, S. Ramaprabhu, J. Phys. Chem. C 116 (2012) 14179–14187.
[22] T.Y. Kim, H.W. Lee, M. Stoller, D.R. Dreyer, C.W. Bielawski, R.S. Ruoff, K.S. Suh, ACS Nano 5 (2010) 436–442.
[23] D.R. McFarlane, J. Sun, J. Golding, P. Meakin, M. Forsyth, Electrochim. Acta 45 (2000) 1271–1278.
[24] D.C. Marcano, D.V. Kosynkin, J.M. Berlin, A. Sinitskii, Z. Sun, A. Slesarev, L.B. Alemany, W. Lu, J.M. Tour, ACS Nano 4 (2010) 4806–4814.
[25] S. Park, J. An, J.R. Potts, A. Velamakanni, S. Murali, R.S. Ruoff, Carbon 49 (2011) 3019–3023.
[26] A.-L. Pont, R. Marcilla, I. De Meatza, H. Grande, D. Mecerreyes, J. Power Sources 188 (2009) 558–563.
[27] A.M. O'Mahony, D.S. Silvester, L. Aldous, C. Hardacre, R.G. Compton, J. Chem. Eng. Data 53 (2008) 2884–2891.
[28] J. Tang, W. Sun, H. Tang, M. Radosz, Y. Shen, Macromolecules 38 (2005) 2037–2039.
[29] B. Jia, L. Zou, Carbon 50 (2012) 2315–2321.
[30] J.I. Paredes, S. Villar-Rodil, P. Solís-Fernández, A. Martínez-Alonso, J.M.D. Tascón, Langmuir 25 (2009) 5957–5968.
[31] C. Chen, Q.-H. Yang, Y. Yang, W. Lv, Y. Wen, P.-X. Hou, M. Wang, H.-M. Cheng, Adv. Mater. 21 (2009) 3007–3011.
[32] M.J. McAllister, J.-L. Li, D.H. Adamson, H.C. Schniepp, A.A. Abdala, J. Liu, M. Herrera-Alonso, D.L. Milius, R. Car, R.K. Prud'homme, I.A. Aksay, Chem. Mater. 19 (2007) 4396–4404.
[33] S. Stankovich, D.A. Dikin, R.D. Piner, K.A. Kohlhaas, A. Kleinhammes, Y. Jia, Y. Wu, S.T. Nguyen, R.S. Ruoff, Carbon 45 (2007) 1558–1565.
[34] X. Lu, H. Dou, B. Gao, C. Yuan, S. Yang, L. Hao, L. Shen, X. Zhang, Electrochim. Acta 56 (2011) 5115–5121.
[35] L.J. Cote, R. Cruz-Silva, J. Huang, J. Am. Chem. Soc. 131 (2009) 11027–11032.
[36] T.T. Tung, T.Y. Kim, J.P. Shim, W.S. Yang, H. Kim, K.S. Suh, Org. Electron. 12 (2011) 2215–2224.
[37] C.-C. Yang, S.-T. Hsu, W.-C. Chien, J. Power Sources 152 (2005) 303–310.
[38] M.D. Stoller, R.S. Ruoff, Energy Environ. Sci. 3 (2010) 1294–1301.
[39] Z. Lei, N. Christov, X.S. Zhao, Energy Environ. Sci. 4 (2011) 1866–1873.
[40] C.-T. Hsieh, S.-M. Hsu, J.-Y. Lin, H. Teng, J. Phys. Chem. C 115 (2011) 12367–12374.
[41] C. Portet, P.L. Taberna, P. Simon, C. Laberty-Robert, Electrochim. Acta 49 (2004) 905–912.
[42] L. Cao, F. Xu, Y.Y. Liang, H.L. Li, Adv. Mater. 16 (2004) 1853–1857.
[43] M. Sun, G. Wang, X. Li, C. Li, J. Power Sources 245 (2014) 436–444.
[44] M.-T.F. Rodrigues, P.M. Ajayan, G.G. Silva, J. Phys. Chem. B 117 (2013) 6524–6533.